DOI: 10.1002/fuce.201700128

Numerical Study of Solid Oxide Fuel Cell Contacting Mechanics

Z. Chen[1]*, X. Wang[2], N. Brandon[1], A. Atkinson[2]

[1] Department of Earth Science and Engineering, Imperial College, ■city??■ SW7 2BP, UK
[2] Department of Materials, Imperial College, ■city??■ SW7 2BP, UK

Received July 07, 2017; accepted December 05, 2017; published online ■■■

Abstract

Assembly of a planar SOFC or SOE stack involves the lamination of cells and interconnect plates under an applied load. In most designs a pattern of ribs on the interconnector makes contact with a porous ceramic current collector layer on the air side. These localised contacts are regions of increased stress on the cells and can cause damage if the stresses become too large. In this paper the mechanical response of an anode-supported cell to localised loads from interconnector ribs is simulated. The simulations show that the critical stress for initiating and propagating a crack in the electrolyte (~300MPa for a 10 μm thick electrolyte) is reached when the interconnector displacement reaches 20 μm (after touching the cathode) with reduced support, or 30 μm when in an oxidized state. The difference is due to the lower stiffness of the reduced support. The residual compressive stress in the electrolyte layer has a major protective effect for the electrolyte. It is concluded that fracture is very unlikely for a geometrically perfect contact, but if the contact is non-uniform due to manufacturing variability in the contact plate or cell, local displacements >~20 μm can be dangerous. The simulations are used in an example of contacting geometry optimisation.

Keywords: Contacting; Electrolyte Fracture, Finite Element Modeling (FEM), Optimization, Solid Oxide Fuel Cell (SOFC)

1 Introduction

All SOFC and SOE devices require electronic current collection to the electrodes. In stacks of planar cells this involves making a contact between the electrode and the interconnector or bipolar plate. On the fuel side this is usually achieved using a nickel mesh or nickel felt. On the air side, the contact is usually made between ribs on the interconnector and the porous air electrode itself, or a similar porous ceramic current collector layer [1]. When the stack is assembled forces are applied to compress the stack, for example by tie-bars between relatively stiff end plates. This applied load serves to accommodate deviations from cell flatness and control or compress seals. It also pushes the interconnector ribs into the air electrode to make the current collection contact [2]. In this respect, the externally applied force becomes a local load where the interconnector rib contacts the air electrode. The average pressures used in stack assembly are usually small: e.g. 1 MPa for a stack with glass seals, up to 20 MPa for compressible seals [3]. However, if the components making contact are not perfectly flat or smooth due to manufacturing variability, then the loads can be magnified considerably at the initial places of contact. Penetration of the rib into the electrode structure is beneficial as it improves contact and also accommodates some variations in manufacturing tolerances. However, if the local load becomes too high it can cause damage to the cell. This is a particular risk for cell structures having a thin electrolyte layer such as anode-supported SOFCs. Fracture of the electrolyte can allow direct combustion of fuel and air during operation, leading to a local hot-spot and eventual destruction of the cell. As the interconnector rib makes contact with the cathode (in a SOFC) it compresses the cathode leading to collapse of the porous ceramic structure and its local densification. The load is transferred downwards deforming the electrolyte layer and eventually the anode support, which is also porous and capable of densification.

The aim of the current work is to study the mechanics of this process by finite element (FE) simulation of the cell contacting and to identify a suitable criterion for preventing damage to the electrolyte in an anode-supported cell (ASC). The approach adopted involves applying results of previous indentation experiments and FE simulations of the local loading of the cell component materials and layered structures [4, 5]. Particular attention is given to a suitable description of the collapse and densification of the porous materials under compressive loading and the criterion for failure of the electro-

[*] *Corresponding author, chen@ic.ac.uk*

lyte. The results are then used in a FE simulation of contacting between an ASC cathode and an interconnector rib. In this simulation the anode support is considered to be perfectly supported on its lower surface and not able to bend under the localised load at the cathode surface. This might not be the case in an actual stack and depends on the details of the anode-side current collection and stack design. Any bending of the cell will help reduce the cathode side contact stresses. This can also occur if there is misalignment of connector ribs on the anode and cathode sides of the cell. Therefore this simulation represents a worst-case scenario for contact damage to the electrolyte, but the longer range bending stresses could threaten the integrity of the support.

The simulation is also used as an example in a design of experiment analysis using the Taguchi method to explore optimisation of the rib geometry from the point of view of minimizing the stress in the electrolyte.

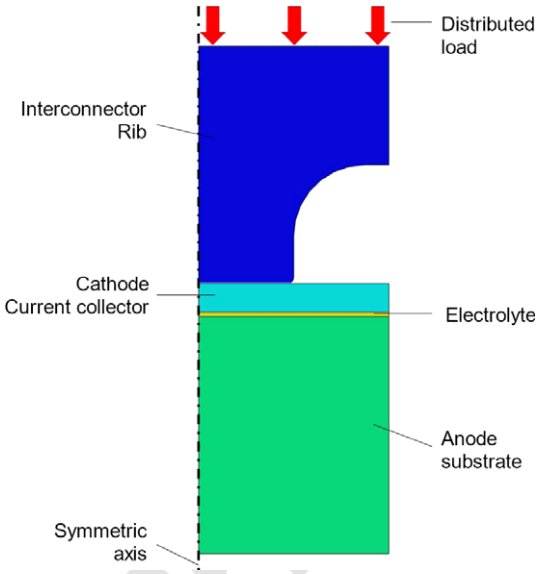

Fig. 1 Schematic of symmetrical and periodic model setup under plane strain condition.

2 Simulation Procedure

2.1 Finite Element Model

As an example of the application of data obtained in earlier studies, FE simulations were performed to simulate the contact behavior between an anode-supported SOFC and an interconnector rib, as shown in Figure 1, with properties of the components listed in Table 1. A 2D plane strain FE model was used in Abaqus CAE 6.12 environment (Dassault Systemes, USA). The structure was assumed periodic with a vertical plane of symmetry at the center of the rib. This corresponds to a large area interconnector and cell (all edge effects ignored) with perfectly flat and smooth surfaces. The simulations are in plane strain and are invariant in the third dimension (along the direction of the ribs). A sandwich-shaped three-layer model was built for the cell comprising a thin (10 µm for the base case) dense electrolyte layer on a porous anode substrate (oxidized or reduced states) having much larger thickness (500 µm). On top of the electrolyte layer a porous LSCF cathode layer sintered at 1,000 °C was built (30 µm thick in the base case). The width of the semi-repeating unit was set at 200 µm. The interfaces between the layers were assumed perfectly bonded (i.e. no delamination or slippage allowed). In reality, cells often contain other layers, such as a thin (e.g. 5 µm) anode functional layer between the support and the electrolyte. For simplicity, such a layer is not included here as it is relatively thin compared with the support and has similar composition (although a finer microstructure) and would have very similar mechanical properties to the support.

The schematic of the model is shown in Figure 1. The bottom of the anode substrate was constrained to not allow vertical movement (U2 = 0). All the edges on the symmetric axis for all parts were constrained such that no horizontal movement was allowed (U1 = 0). The periodicity required additionally that the edges on the right hand side of each part were constrained to have the same horizontal displacement (U1) during loading and unloading. The dimensions of the individual parts for the base case are listed in Table 1.

Adaptive meshing was employed in the regions close to the rib contact edge in order to improve the resolution of the stress distribution in that critical region. A mesh convergence analysis was performed to test the mesh size sensitivity of the results and ensure that the results were not dependent on the

Table 1 Material properties and base case dimensions of the model.

Component	Thickness /µm		Material	Elastic modulus / GPa	Gurson yield stress / GPa	Porosity	Residual stress /GPa
Anode support	500		NiO-8YSZ	151	3	0.146	
			Ni-8YSZ	80	0.96	0.301	
Electrolyte	10		YSZ	219	–	0	–0.6 (oxidized) and –0.4 (reduced)
Cathode	30		LSCF	44.5	0.9	0.363	0.1
Metallic rib	height	Width	Crofer® 22 APU [3]	220	0.27[a]	–	–
	500	400					

(a) von Mises yield stress for the interconnector steel

mesh resolution. A uniformly distributed load was applied on the top surface of the interconnector plate by means of a rigid flat plate constrained to have displacement only in the vertical direction. The loading and unloading processes were simulated by stepwise vertical displacement of the rigid plate into and off the structures.

2.2 Input Material Properties

The mechanical properties shown in Table 1 for these components were measured previously using spherical indentation experiments [5–7]. The properties for the porous cathode layer are appropriate for one sintered at 1,000 °C. Typical SOFC porous NiO-8YSZ anode substrates (oxidized condition) of approximately 500 μm thickness with a 10 μm 8YSZ electrolyte on one side were used. Comparison was also made with the model when the oxidized anode substrate was fully reduced to Ni-8YSZ.

The material of the interconnector rib was assumed to be Crofer® 22 APU (ThyssenKrupp VDM GmbH) ferritic stainless steel, for which the mechanical properties [8] are also shown in Table 1. The cell materials were assumed to be homogeneous and isotropic.

A key feature of the simulation is the way it deals with collapse and densification of the porous materials. This was done using the Gurson model [9] in which the yield condition is a function of the porosity (f) and is given by the following expression, Eq. (1),

$$\Phi = \left(\frac{q}{\sigma_y^d}\right)^2 + 2f\cosh\left(-\frac{3p}{2\sigma_y^d}\right) - 1 - f^2 = 0 \quad (1)$$

where σ_y^d is the yield stress of the dense matrix material, q is the effective von Mises macroscopic stress and p is the macroscopic hydrostatic stress. Since we apply this relationship outside the limits of its strict validity we treat σ_y^d as an adjustable parameter whose value is obtained by a best fit to the indentation response of the porous material (this is not necessarily the same as the yield stress of the dense matrix). This is the Gurson yield stress shown in Table 1 and was determined for the individual materials in the cell from fitting loading and unloading spherical indentation experiments and verified by post-test characterization of deformed regions after indentation. Details can be found in [5–7].

For the non-porous metallic interconnector the von-Mises yield criterion was used for the onset of plastic deformation,

$$_y = \sigma_{Mises} = \sqrt{\frac{(\sigma_1-\sigma_2)^2 + (\sigma_2-\sigma_3)^2 + (\sigma_3-\sigma_1)^2}{2}} \quad (2)$$

where σ_1, σ_2 and σ_3 are the three principal stresses and σ_{Mises} is the von-Mises stress. The work hardening behavior of the Crofer steel was included in the simulations as a look-up table of true stress, strain and plastic strain converted from nominal engineering stress-strain data provided by the material supplier [8].

In addition, the cathode and electrolyte layers on these substrates are known to have an in-plane equi-biaxial residual stress resulting from thermal expansion differences. The electrolyte residual stresses are -600 MPa in the oxidized state and -400 MPa in the reduced state [10, 11]. The base case residual stress in the cathode, for which no measurements were available, was estimated assuming elastic behavior using Eq. (3)

$$\sigma_{thermal} = \frac{E}{1-\nu^2}(\alpha_f - \alpha_s)(T_0 - T) \quad (3)$$

where α_f and α_s are TEC of the thin layer and thick substrate and E and ν are the elastic modulus and Poisson's ratio of the thin layer. T_0 is the stress free temperature, which is regarded as being close to, but slightly below, the sintering temperature, and T is room temperature (25 °C). The residual stresses were incorporated in the simulations as initial conditions. The balancing stress in the substrate is much smaller (because it is much thicker than the electrolyte or cathode) and was neglected.

The friction coefficient between metal and cathode was assumed to be 0.5, which is a commonly assumed value for similar contacting surfaces. The friction coefficient (μ) at the interface between the rib and cathode interface was varied to see how much it would affect the simulated stress distributions. The base case value of μ was set at 0.5, and a smaller μ (= 0.1) was then used for comparison for both the oxidized and reduced cases. It was found that the friction coefficient has a significant effect on the stress distributions. When the friction coefficient was reduced to 0.1 there was noticeably more plastic deformation of the metal and greater displacement of the edge of the rib towards the gas channel. The maximum tensile stress in the electrolyte was also reduced significantly and its location displaced towards the center of the rib. However, the maximum vertical displacement of the electrolyte remained almost unaffected. Although these results show that the friction coefficient has a large influence on the stress distribution, the value of 0.1 is unlikely to be encountered in a contact involving a granular porous ceramic and therefore the base case value of 0.5 should be more representative of a real situation.

2.3 Design Optimisation Using the Taguchi Method

For the two types of specimen (oxidized and reduced), three parameters were varied from the base case values in Table 1 to examine their effects on the electrolyte stress. They are rib edge curvature radius (R), cathode thickness (CT) and electrolyte thickness (ET), as listed in Table 2. The Taguchi design of orthogonal experiments method [12] was used to perform a series of simulations to identify the importance of these factors and the optimal values for the three factors, aiming to generate the lowest peak maximum principal stress (S_{max}) in the thin electrolyte layer.

Table 2 Factors, levels and values for the Taguchi optimisation. Factors are: rib edge curvature radius (R), cathode thickness (CT) and electrolyte thickness (ET).

Factor	Level 1	Level 2	Level 3
R / μm	12.5	25	50
CT / μm	15	30	60
ET / μm	5	10	20

The base case simulations suggested that suitable applied loads of 170 mN and 120 mN, for the oxidized and reduced supports were appropriate. Therefore, all the orthogonal simulations are based on these fixed loads. However, the values of the variable parameters (factors) were the same for both oxidized and reduced cases.

Three value levels were used for each factor as shown in Table 2. In all cases the range of each is a factor of 4 and the values are typical of those used in actual cells. In this study, a 3×9 experimental array was adopted as shown in the orthogonal table (Table 3).

The range analysis method was used to analyze and interpret the results from the design of experiments. The optimum levels of each factor were finally chosen to achieve the lowest value of S_{max} in the electrolyte.

3 Results and Discussion

3.1 Critical Stress for Electrolyte Fracture

In order to determine whether a particular peak stress in the electrolyte is likely to cause fracture, it is necessary to have a suitable criterion for failure. Brittle failure of ceramics involves first the initiation of a crack (e.g. at a defect or sharp geometrical feature) and then propagation of the crack driven by the stress field, which changes as the crack propagates. The initiation is usually described in terms of a critical value of stress (strength, σ_c) and the propagation by a critical energy release per unit area of crack extension, G_c. For fracture the conditions for both initiation and propagation must be satisfied, but often it is one that dominates. The strength depends on the distribution of flaws and the probability that a critical flaw exists in the stressed volume. The result is that the strength decreases as the stressed volume increases. For any initiating defect, or propagating crack, the opening mode tensile stress is the most significant and therefore, from the FE simulations, the key parameter is the maximum principal stress in the complicated stress field near the contact.

In our previous study of damage to an electrolyte layer caused by spherical indentation [5] the critical stress for electrolyte fracture was estimated from its known fracture toughness and the observed defects which were of the order of 1 μm in size. This is not a suitable critical stress for the current analysis because the volume of electrolyte stressed by the rib is much greater than for the spherical indenter and therefore the chance of finding a larger defect in also greater. Since the electrolyte is thin there will be a limit to the size of a pre-existing defect. To obtain an estimate for the critical stress we assume that the maximum credible defect is a short crack penetrating from the top surface to the middle of the electrolyte. Under a tensile component of stress in the plane of the electrolyte this pre-existing crack could be initiated to penetrate the intact half of the electrolyte. This problem was analyzed theoretically by Beuth [13]. The expression relating critical stress for initiation of fracture, σ_{in}, to the Mode I critical stress intensity, K_{Ic}, takes the form

$$\frac{K_{Ic}}{\sigma_{in}(\pi h)^{1/2}} = F\left(\alpha, \beta, \frac{a}{h}\right) \tag{4}$$

In this expression h is the film thickness and a the depth of the crack. Therefore, for an initial defect penetrating to the middle of the film a/h = 0.5. α and β are the Dundurs parameters for the elastic mismatch at the interface between film and substrate. The approximate values for the oxidized support are α = 0.18 and β = 0.05, and for the reduced support α = 0.46 and β = 0.13. The value of F was calculated numerically by Beuth as a function of these parameters and is approximately equal to 1 for both supports. For 8YSZ K_{Ic} = 1.61 MPa m$^{1/2}$ [14] and therefore Eq. (4) predicts a critical stress for initiation of 290 MPa.

Beuth also considered the lateral propagation of a crack traversing the film, a so-called channelling crack. When longer than a few times the film thickness the energy release rate (with respect to increase in crack length) as the crack extends laterally is constant and given by

Table 3 Simulation ''experiments'' for the Taguchi optimisation applied to the oxidized and reduced cases.

Experiment no.	Input factors and levels			Simulation values		
	R	CT	ET	Radius / μm	Cathode thickness / μm	Electrolyte thickness / μm
1	1	1	1	12.5	15	5
2	1	2	2	12.5	30	10
3	1	3	3	12.5	60	20
4	2	1	2	25	15	10
5	2	2	3	25	30	20
6	2	3	1	25	60	5
7	3	1	3	50	15	20
8	3	2	1	50	30	5
9	3	3	2	50	60	10

$$G = \frac{1}{2}\frac{\sigma^2(1-\nu^2)h}{E}\pi g(\alpha,\beta) \quad (5)$$

where E and ν refer to the film. The function g was also computed numerically by Beuth and has the value 1.48 for the materials in these cells. Furthermore, in plane strain,

$$K_I^2 = \frac{EG}{1-\nu^2} \quad (6)$$

and hence the final result is that the critical stress for crack propagation as a channel crack in 1.16 times the critical stress for initiation, or σ_{prop} = 1.16σ_{in} = 336 MPa. Since the values of critical stress for both initiation and propagation are so similar a suitable failure criterion is that a maximum principal stress of approximately 300 MPa would lead to electrolyte failure.

3.2 Examples of Stress Distributions

Figure 2 shows examples of stress distributions at applied loads that are just sufficient to reach the elastic limit of the interconnector steel. This is when the von Mises stress in the steel reaches the yield stress of 270 MPa, which is seen to occur initially at the corner of the rib in contact with the cathode. The mean pressure on the interconnector plate is obtained by dividing the applied load by the total area of the top of the interconnector plate and is higher for the oxidized support because the support is stiffer than when reduced. Since in this case the width of the rib is one half of the repeat unit then the mean contact pressure is double the mean pressure.

Also shown in Figure 2 is the maximum principal stress in the electrolyte, which never becomes tensile as the residual compressive stress is not overcome. Therefore, it is concluded that plastic deformation of the interconnector will always occur before there is any danger of damage to the electrolyte in this particular case.

Further simulations were carried out to explore the stress distributions for higher mean pressures than those in Figure 2 and which would generate electrolyte stresses of the order of the failure stress of 300 MPa. Figure 3 shows the distribution of the maximum principal stress (note that "maximum principal stress" respects the normal sign convention of tensile stress being positive) and the vertical displacement (U2) for the oxidized and reduced specimens computed in the FE simulations in the absence of any cracking at mean pressures of 0.78 GPa and 0.63 GPa respectively. It can be seen from Figure 3 that these pressures are sufficient to cause plastic deformation of the metal interconnector, especially in the case of the oxidized support. The general form of deformation of the electrolyte layer is biaxial bending due to the less stiff substrate, which occurs to a similar degree (as seen from the similar displacement of the electrolyte beneath the rib), but at a lower applied pressure, for the reduced support. The maximum principal stress in the electrolyte is found at a location just outside the edge of the contact.

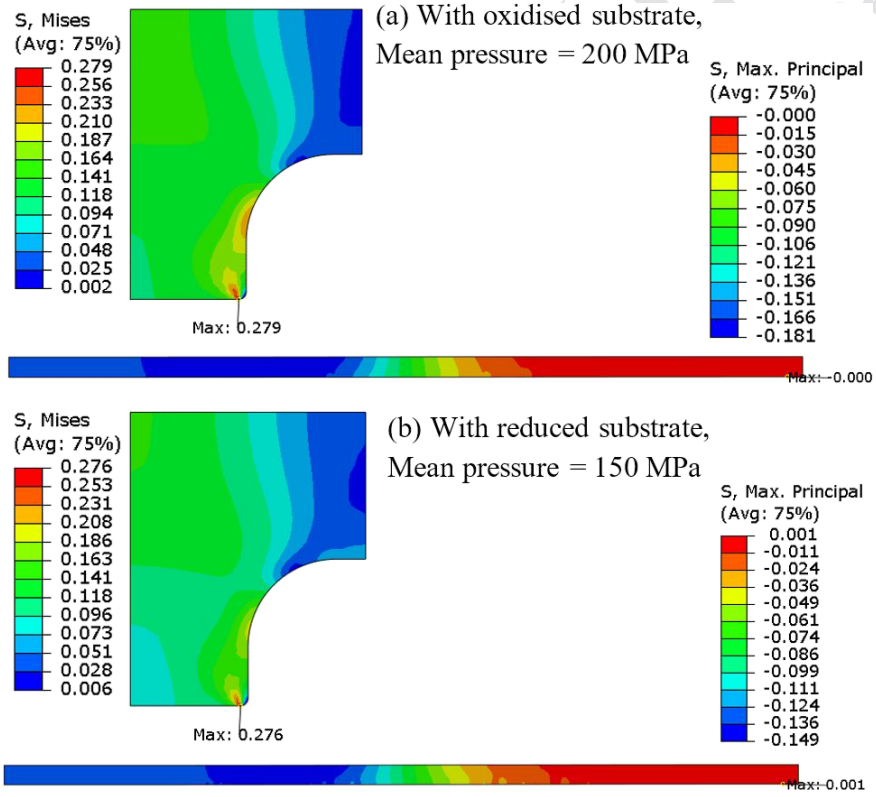

Fig. 2 Stress distributions (in GPa) from FE simulation in the (a) oxidized and (b) reduced states at applied loads corresponding to the onset of yielding (plastic deformation) of the rib. The maximum principal stress in the electrolyte is shown in the lower part of each figure.

3.3 Stress Gradient Across the Electrolyte Thickness

In order to interpret the maximum stresses in the stress distributions in terms of the critical stress for electrolyte failure it is necessary to determine the spatial extent of the high stress region and particularly whether the high stress extends across the electrolyte thickness. This is because in estimating the failure stress it was assumed that the electrolyte was under a uniform applied stress. An example of the variation in maximum principal stress across the electrolyte thickness at the location of maximum tensile stress stresses is shown in Figure 4 for the same loading mean pressures as used in Figure 3. The plot shows that although the maximum principal stress decreases by approximately 30–40% across the electrolyte thickness, the assumption of a constant stress is reasonable considering the other simplifying assumptions made in estimating the failure stress. A related

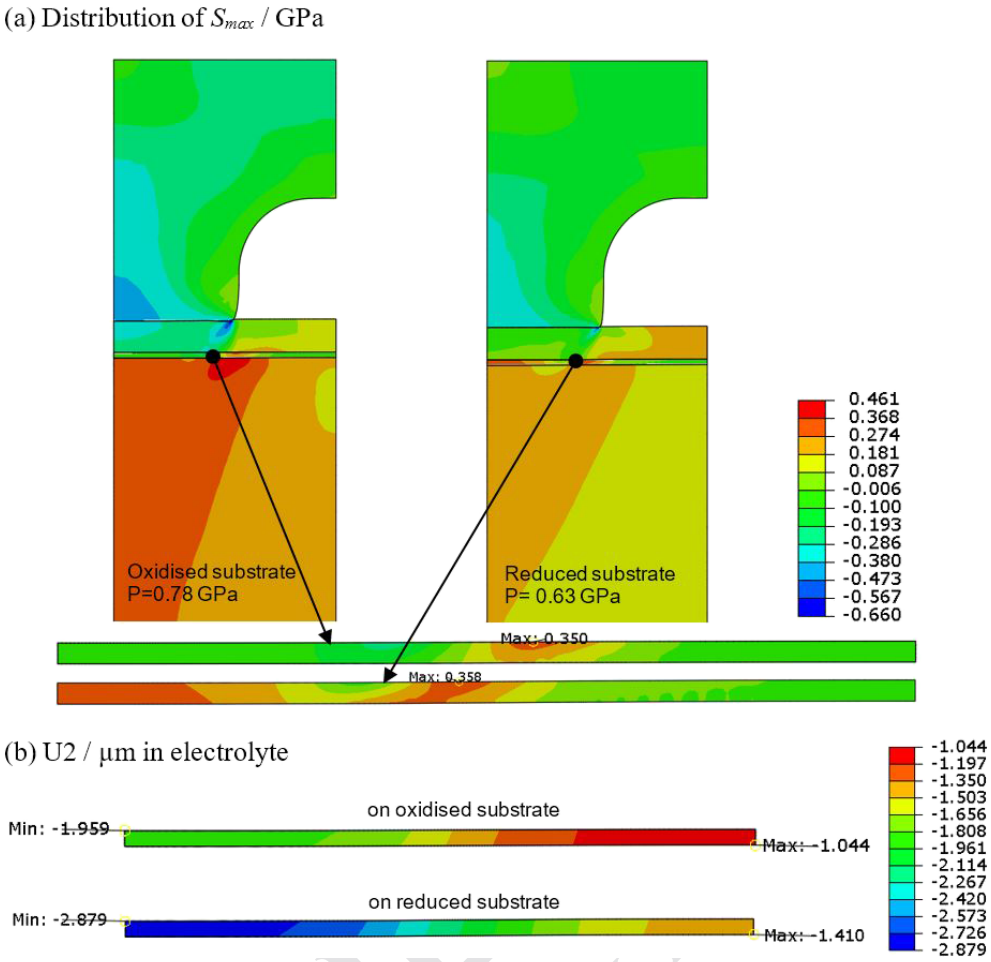

Fig. 3 (a) Maximum principal stress distribution and (b) vertical displacement (U2) in the electrolyte, for simulations with oxidized and reduced supports, at applied mean pressures giving a maximum principal stress of ~0.350 GPa in the electrolyte (mean applied pressure: 0.78 GPa and 0.63 GPa, respectively, friction coefficient = 0.5).

issue concerns the lateral extent of the maximum stress when considering crack propagation as a channel crack. The contour plots in Figure 3 indicate that the lateral extent of the high stress region has a lateral extent of a few multiples of the electrolyte thickness. As a channel crack propagates in a film, the crack relaxes the stress (and releases the stored energy) over a distance of the same order as the film thickness. Thus the pre-existing stress outside of this region has no influence on the propagation of the channel crack except to constrain its direction to remain within the high stress region. Therefore, it can be concluded that the stress distribution in the high stress region is sufficiently uniform for the estimation of critical stresses for initiation and propagation of electrolyte cracks to be reasonable and that the failure mode will be a crack initiating close to the edge of the contact rib and propagating along the direction of the rib.

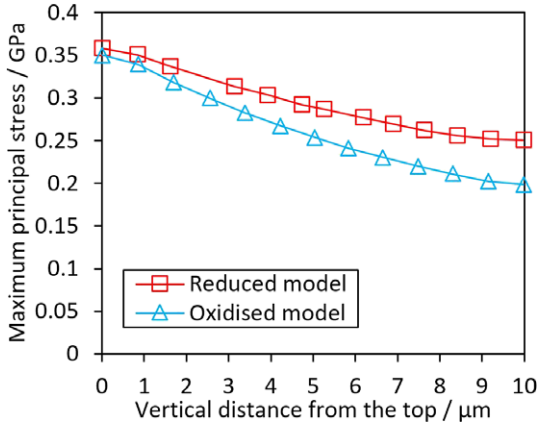

Fig. 4 Maximum principal stress across the electrolyte layer thickness at the location of the peak maximum principal stress.

3.4 Sensitivity of Peak S_{max} to Applied Load

The relationship between the peak maximum principal stress and the applied mean pressure is plotted in Figure 5 (a). It shows that a threshold pressure, is required to overcome the residual compressive stress in the electrolyte, but for pressures above the threshold the peak tensile stress in the electrolyte increases rapidly with applied pressure. The threshold pres-

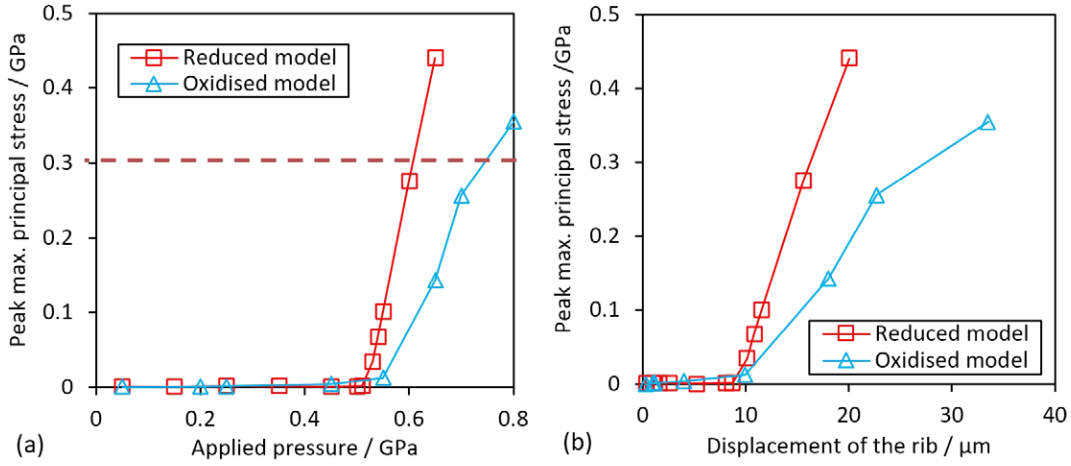

Fig. 5 (a) Peak maximum principal stress in the electrolyte layer as a function of applied mean pressure and (b) the vertical displacement of the interconnector plate top surface. The broken line indicates the estimated critical stress for fracture of the electrolyte layer.

sure is of a similar magnitude to the residual compressive stress and is insensitive to whether the support is oxidized or reduced. However, above the threshold the reduced substrate shows to a much faster increase of stress with applied pressure, as expected from its lower stiffness. The dashed line in Figure 5 (a) indicates the estimated critical stress for failure of the electrolyte and shows that once the threshold pressure is exceeded only a relatively small extra pressure of 100 (reduced support) to 200 MPa (oxidized support) is required to fracture the electrolyte.

Figure 5 (b) shows the peak maximum principal stress in the electrolyte as a function of the displacement of the top surface of the interconnector plate. It has a similar form to the plot in Figure 5 (a) and shows that a displacement of approximately 10 µm is required to overcome the compressive residual stress and a total of approximately 20 µm to reach the critical stress for fracture of the electrolyte on the reduced support, or 30 µm on the oxidized support.

3.5 Sensitivity of Peak Electrolyte Stress to Residual Stress in Cathode and Electrolyte

The sensitivity of peak maximum principal electrolyte stress on the residual stress in cathode and electrolyte layers is plotted in Figure 6 (a) and (b), for oxidized and reduced models, respectively. The residual stress in the cathode layer was varied from 0 to 1,000 MPa (tensile), while fixing the residual stress in the electrolyte at –600 MPa for the oxidized support or –400 MPa for the reduced support. Similarly, the residual stress in the electrolyte was varied from –1,000 to 0 MPa (compressive), while the residual stress in the cathode layer was fixed at 100 MPa.

The results show that the residual stress in the cathode layer has very little influence on the peak maximum principal stress in the electrolyte layer. Conversely the peak maximum principal stress in the electrolyte layer is linearly dependent on the residual stress in the electrolyte layer as a direct consequence of the compressive residual stress acting in opposition to the tensile stress induced by the applied pressure.

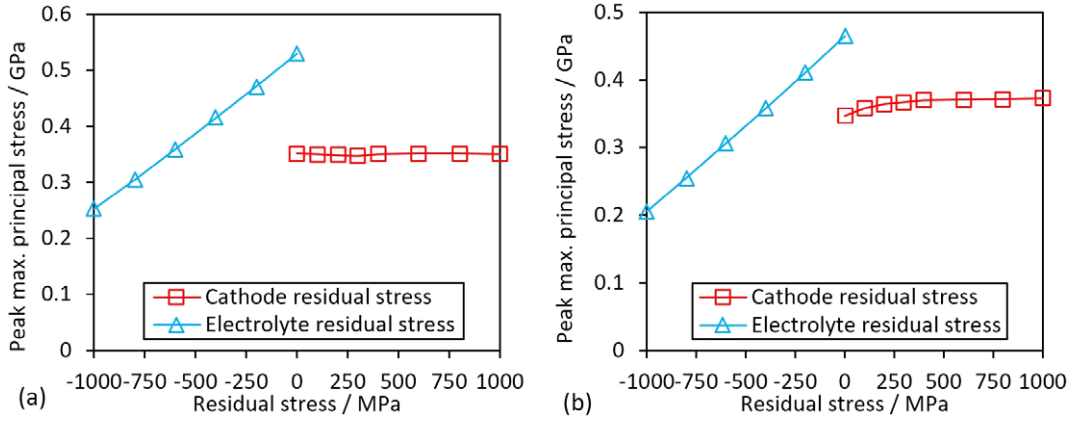

Fig. 6 Peak maximum principal stress in the electrolyte layer as a function of the residual stress in the cathode and electrolyte layers for (a) oxidized support and (b) reduced support.

3.6 Implications for Dimensional Tolerance of Stack Components

The mean applied pressure in a stack depends mainly on the method of sealing at the edges of cell components. In many cases when glass/ceramic seals are used the mean pressures on the stack are of the order of only 1 MPa [2]. When deformable high temperature gaskets are employed these generally require higher mean pressures on the seal of typically 20 MPa [3], although hybrid versions (combined with a glass coating) have been developed requiring seal pressures below 1 MPa [15]. The simulation results show that for a perfectly manufactured cell and interconnector plate, much larger mean applied pressures are required in order for the peak maximum principal stress in the electrolyte to reach a level that is likely to cause fracture of the electrolyte. This is due in large part to the protective effect of the residual compressive stress in the electrolyte. As a result, it is extremely unlikely that electrolyte fracture would occur for such geometrically perfect components.

However, real cells and interconnector plates are not perfect; they can have thickness variations or deviations from flatness, e.g. waviness. The question arises regarding how large a deviation from geometric perfection can be tolerated without fracturing the electrolyte. If initial contact is made locally, the local contact pressure can be much greater than the mean pressure on the stack by a factor equal to the area of the stack plane divided by the area of the local contact. In terms of displacement, rather than pressure, the results in Fig. 5 (b) indicate that a displacement of the interconnector plate of approximately 20 µm, relative to the plane of the base of the support, is required to reach the critical stress for fracture of the electrolyte on the reduced support, and 30 µm on the oxidized support. It can therefore be estimated that in order not to risk fracture of the electrolyte due to a local contact, the components should be flat to less than approximately 20 µm.

The data used in the simulations described above relate to formation of the contact at room temperature. When glass/ceramic seals are used the contact is formed at a temperature slightly above the design operating temperature and, even with compressive seals, a pressure is maintained during operation. At typical operating temperatures (500 to 800 °C) the material properties are different and time dependent deformation due to creep must also be considered. In general, the elastic moduli, yield stress and fracture stress will all be lower at higher temperature. In addition, residual stresses are relaxed and, in particular for anode supported cells, the protective compressive stress in the electrolyte will be relaxed. Therefore, it is not possible to conclude, based on the present simulations and input data, whether electrolyte fracture is more, or less, likely at operating temperature.

3.7 Results of the Design of Experiments (DoE)

The results for peak maximum principal stress, S_{max}, from simulations using the input parameters shown in Table 3 were analyzed using the direct analysis method to find the optimum parameter combination for minimizing S_{max}. This (Figure 7) showed that the lowest value of S_{max} would be obtained with an edge radius of 50 µm, cathode thickness of 15 µm and electrolyte thickness of 20 µm for the oxidized substrate, and radius of 12.5 µm, cathode thickness of 15 µm and electrolyte thickness of 20 µm for the reduced substrate.

When interpreting these results with respect to the electrolyte thickness it is important to bear in mind that minimizing the peak maximum principal stress in the electrolyte can be misleading when the objective is to avoid electrolyte failure. This is because the critical failure stress decreases in inverse proportion to the square root of the electrolyte thickness according to Eqs. (4) and (5). Thus the thinner the electrolyte the more likely it is to survive, as well as contributing a lower ohmic resistance to the cells.

4 Conclusions

When a contact is made between a ribbed interconnector plate and an anode supported SOFC under an externally applied load, the electrolyte layer is deformed in bending and tensile stresses are developed just outside the edge of the contact rib. If the mean applied pressure is sufficiently high, then

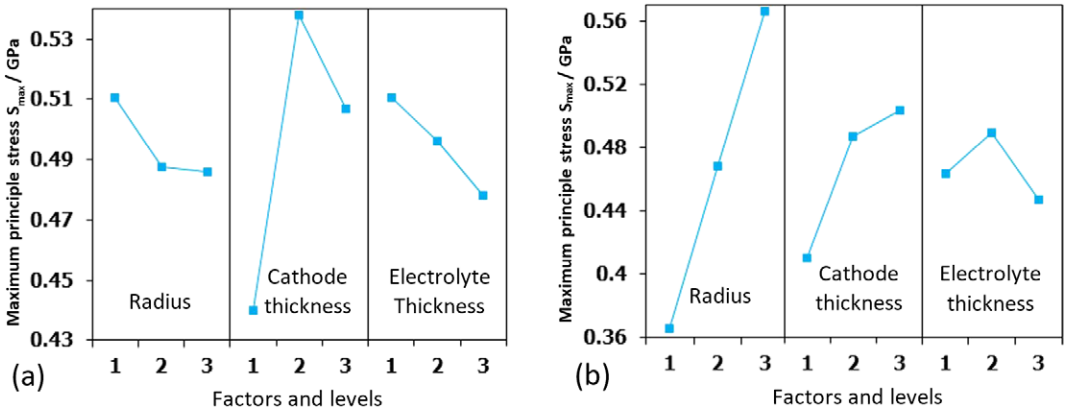

Fig. 7 Average degree of influence on the peak value of maximum principal stress for each factor in the optimisation, for (a) oxidized support and (b) reduced support. The numbers 1, 2 and 3 indicate the levels for each factor which take the values given in Table 2.

there is a risk of fracturing the electrolyte and propagating a crack parallel to the rib direction. For a typical 10 μm thick YSZ electrolyte layer the critical stress for initiating and propagating such a crack is estimated to be approximately 300 MPa. (The critical fracture stress depends on the electrolyte thickness and is inversely proportional to the square root of the thickness). FE simulations show that the mean applied pressure required to induce a stress of this magnitude is approximately 700 MPa when the anode support is in an oxidized state and 600 MPa when in a reduced state. The difference is due to the lower stiffness of the reduced support which allows easier bending of the electrolyte layer. The residual compressive stress in the electrolyte layer has a major beneficial protective effect for the electrolyte and a mean applied pressure of approximately 500 MPa is required in a typical case to overcome this compressive stress. The critical mean pressure for electrolyte fracture is so high that fracture is very unlikely for a geometrically perfect contact. However, this is not the case if contact preferentially occurs at one rib due to variability in geometry due to manufacturing. In such a case the critical out of flatness tolerance is estimated to be approximately 20 μm, above which there is a danger of fracturing the electrolyte.

Other geometric parameters such as the corner radius of the rib, the thickness of the cathode, the residual stress in the cathode and the electrolyte thickness do not have a major influence on the maximum tensile stress in the electrolyte. However, thinner electrolyte layers are beneficial because the critical stress for fracture is higher.

The materials data used in the simulations are appropriate for room temperature. At higher temperatures the materials will have different (usually inferior) mechanical properties, creep deformation is possible and residual stresses will be relaxed. Therefore, the conclusions cannot be applied to stack loading at high temperature without further detailed simulations.

The failure mode analyzed here is electrolyte fracture because its consequence is gas leakage across the cell. The support is much thicker than the electrolyte and the contact stresses in it are of short range, so any damage will not compromise the cell. However, if the cell can bend then the support could fail from tensile stress on its lower surface. Such a scenario is not addressed in the current study.

Acknowledgement

This research was supported by the Hydrogen and Fuel Cell SUPERGEN Hub under EPSRC grant EP/J016454/1, and the Electrodes by Design project under EPSRC grant EP/M014045/1. The authors are grateful to Dr N. Menzler of Forschungszentrum Jülich for provision of specimens.

References

[1] L. Blum, G. J. D. Haart, J. Malzbender, N. H. Menzler, J. Remmel, R. Steinberger-Wilckens, *J. Power Sources* **2013**, *241*, 477.
[2] L. Blum, *Electrochim. Acta* **2017**, *223*, 100.
[3] J. Hoyes, M. Rautanen, *ECS Transactions* **2013**, *57 (1)*, 2365.
[4] Z. Chen, X. Wang, N. Brandon, A. Atkinson, *J. Euro. Ceram. Soc.* **2017**, *37*, 1031.
[5] Z. Chen, X. Wang, N. Brandon, A. Atkinson, *J. Euro. Ceram. Soc.* **2017**, *37*, 4763.
[6] Z. Chen, X. Wang, V. Bhakhri, F. Giuliani, A. Atkinson, *Acta Mater.* **2013**, *61*, 5720.
[7] Z. Chen, X. Wang, A. Atkinson, N. Brandon, *J. Euro. Ceram. Soc.* **2016**, *36*, 1435.
[8] ThyssenKrupp VDM GmbH, Crofer_22_APU Data Sheet, can be found under http://www.vdm-metals.com/fileadmin/user_upload/Downloads/Data_Sheets/Data_Sheet_VDM_Crofer_22_APU.pdf, **2017**.
[9] A. L. Gurson, *J. Eng. Mat. Tech.* **1977**, *99*, 2.
[10] B. Sun, R. A. Rudkin, A. Atkinson, *Fuel Cells* **2009**, *9*, 805.
[11] W. Fischer, J. Malzbender, G. Blass, R. Steinbrech, *J. Power Sources* **2005**, *150*, 73.
[12] G. Taguchi, Introduction to quality engineering: designing quality into products and processes, Asian Productivity Organization, Tokyo, **1986**.
[13] J. Beuth Jr., *Int. J. Solids Struct.* **1992**, *29*, 1657.
[14] A. Selçuk, A. Atkinson, *J. Am. Ceram. Soc.* **2000**, *83*, 2029.
[15] M. Rautanen, O. Thomann, O. Himanen, J. Tallgren, J. Kiviaho, *J. Power Sources* **2014**, *247*, 243.

